NANO LETTERS
Letter
Cite This: Nano Lett. 2018, 18, 6961−6966
pubs.acs.org/NanoLett

Ultrathin van der Waals Metalenses

Chang-Hua Liu,[*,†,‡] Jiajiu Zheng,[§,⊥] Shane Colburn,[§,⊥] Taylor K. Fryett,[§] Yueyang Chen,[§] Xiaodong Xu,[†,∥] and Arka Majumdar[*,†,§]

[†]Department of Physics, University of Washington, Seattle, Washington 98195, United States
[‡]Institute of Photonics Technologies, National Tsing Hua University, Hsinchu 30013, Taiwan
[§]Department of Electrical and Computer Engineering, University of Washington, Seattle, Washington 98195, United States
[∥]Department of Materials Science and Engineering, University of Washington, Seattle, Washington 98195, United States

Supporting Information

ABSTRACT: Ultrathin and flat optical lenses are essential for modern optical imaging, spectroscopy, and energy harvesting. Dielectric metasurfaces comprising nanoscale quasi-periodic resonator arrays are promising for such applications, as they can tailor the phase, amplitude, and polarization of light at subwavelength resolution, enabling multifunctional optical elements. To achieve 2π phase coverage, however, most dielectric metalenses need a thickness comparable to the wavelength, requiring the fabrication of high-aspect-ratio scattering elements. We report ultrathin dielectric metalenses made of van der Waals (vdW) materials, leveraging their high refractive indices and the incomplete phase design approach to achieve device thicknesses down to $\sim\lambda/10$, operating at infrared and visible wavelengths. These materials have generated strong interest in recent years due to their advantageous optoelectronic properties. Using vdW metalenses, we demonstrate near-diffraction-limited focusing and imaging and exploit their layered nature to transfer the fabricated metalenses onto flexible substrates to show strain-induced tunable focusing. Our work enables further downscaling of optical elements and opportunities for the integration of metasurface optics in ultraminiature optoelectronic systems.

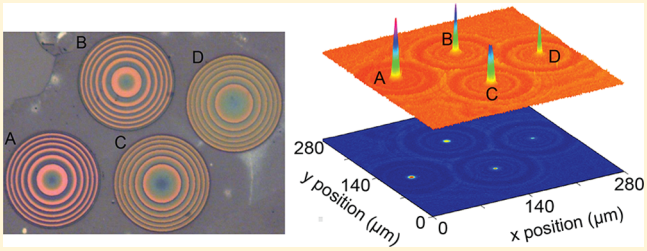

KEYWORDS: *van der Waals nanophotonics, ultrathin dielectric metalens, integrable metalens, tunable metalens, incomplete phase design*

Subwavelength diffractive optical elements, also known as metasurfaces, have fostered considerable interest in the photonics community in recent years.[1−6] A subwavelength scatterer can provide different phase shifts to incident light by virtue of their lateral geometry while having the same thickness. A metasurface exploits this effect to realize ultrathin and flat optical elements, with uniform thickness, which can be fabricated by a single-stage lithography. Although several works in this field have successfully demonstrated metalenses[7,8] and other optical components[2,3,9] using deep sub-wavelength-thick metallic nanoantennas, these devices usually suffer from high absorption loss and strong polarization sensitivity. An alternative approach is to exploit arrays of dielectric resonators.[4,5,10−13] Thus far, a diverse set of low-loss dielectric metasurface optical elements operating in the infrared and visible wavelength ranges have been reported. However, these dielectric elements are much thicker (on the order of the wavelength) to achieve a full 2π phase shift. At the same time, to impart small phase shifts, the resonators need to have narrower lateral dimensions. Because the thickness is uniform for all of the scatterers, some pillars can end up having a high aspect ratio (typically >5). Fabricating these delicate structures while simultaneously keeping a low sidewall roughness is a challenging nanofabrication task and may limit the practical applications of metalenses. Although thinner and efficient dielectric metasurfaces can be ideally realized at near-infrared wavelengths using high-index materials with low absorption loss, such as group III−V compounds like AlGaAs ($n \approx 3.8$) or GaP ($n \approx 3.4$), it is challenging to directly grow these materials on different substrates.

Layered van der Waals (vdW) materials exhibit diverse optoelectronic properties, ranging from wide-band-gap hexagonal boron nitride (h-BN) and excitonic transition-metal dichalcogenides (TMDCs) to semimetallic graphene.[14,15] These materials can be transferred onto any substrate without requiring explicit lattice matching. This presents new opportunities for creating hybrid nanostructures that can simultaneously take advantage of industrial semiconductor manufacturing technologies and benefit from the unique properties of vdW materials.[15−17] In recent years, these materials have been used in conjunction with integrated nanophotonic structures to demonstrate various active devices for short-distance optical communication and energy-harvest-

Received: July 14, 2018
Revised: September 30, 2018
Published: October 8, 2018

DOI: 10.1021/acs.nanolett.8b02875
Nano Lett. 2018, 18, 6961−6966

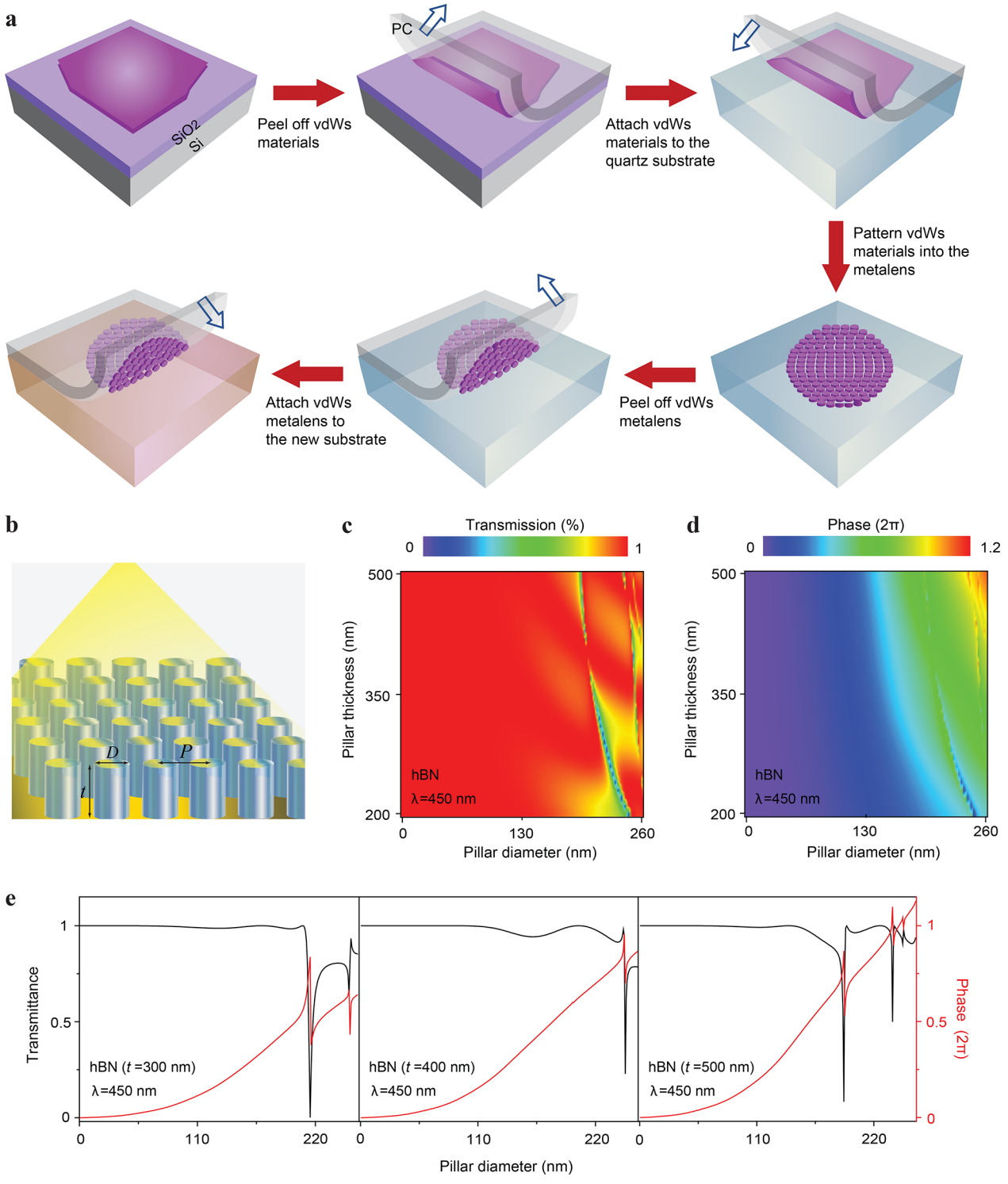

Figure 1. Process of transferring vdW materials and numerical simulations. (a) Schematic diagram shows the nanostructured vdW materials can be transferred onto different substrates using a polycarbonate (PC) film. (b) Schematic illustration of arrays of vdW nanopillars, composed of h-BN and spaced apart by p = 260 nm. Varying the diameter (D) and thickness (t) of the pillars affects the transmission properties of incident light. (c,d) The color maps show RCWA providing the change in the (c) amplitude and (d) phase of a wavefront after passing through the array when varying the dimensions of the nanopillars. (e) Left to right: Pillar diameter versus the change in amplitude (black) and phase (red) of a transmitted wavefront with the thickness of the nanopillars fixed at 300, 400, and 500 nm, respectively. These simulated results are extracted from panels c and d.

ing applications.[14,18−21] Recently, photonic crystal resonators in the visible frequency[22] and nanopatterned periodic subwavelength gratings made of vdW materials at mid-infrared frequencies have been reported,[23] although wavefront engineering in the far-field has not been demonstrated. Additionally, ultrathin Fresnel lenses made of molybdenum disulfide and graphene have been demonstrated.[24,25] These lenses, however, do not exploit nanometer-scale patterning and either

DOI: 10.1021/acs.nanolett.8b02875
Nano Lett. 2018, 18, 6961−6966

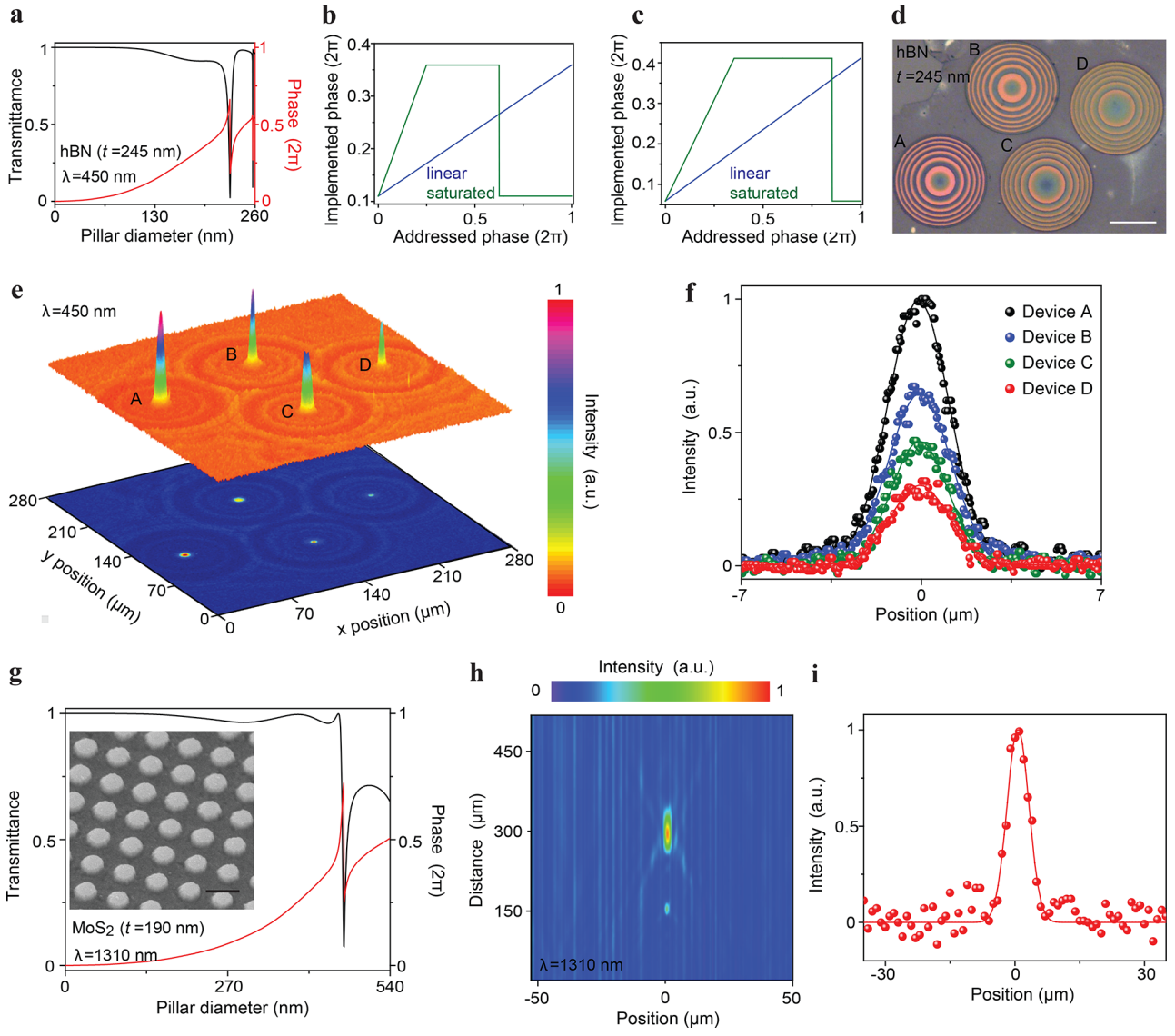

Figure 2. Design principle and characterizations of vdW metalenses. (a) Simulated change in the amplitude (black) and phase (red) of a wavefront passing through a 245 nm thick hBN pillar array. The operating wavelength is 450 nm and the refractive index of hBN is ∼2.17. (b,c) The implemented phase versus the addressed phase is correlated with linear (blue) and saturated (green) mismatched models. The range of implemented phase is (b) 0.22π to 0.72π (diameters ranging from 117 to 195 nm), a total change of 0.5π, and (c) 0.12 to 0.82π (diameters ranging from 90 to 210 nm), a total change of 0.7π. (d) Optical image of the fabricated hBN metalenses captured using the Olympus BX51 microscope. Device A: 0.7π phase modulation and the saturated mismatched model. Device B: 0.5π phase modulation and the saturated mismatched model. Device C: 0.7π phase modulation and the linear mismatched model. Device D: 0.5π phase modulation and the linear mismatched model. Scale bar: 30 μm. (e) Intensity distributions in the focal plane of four metalenses. (f) Line cuts of the intensity distributions along the four focal spots shown in panel e. Their field profiles are fitted to a Gaussian function. The data are normalized with respect to the peak intensity of Device A. (g) Simulated change in the amplitude (black) and phase (red) of a wavefront passing through an array of 190 nm thick MoS_2 pillars with a periodicity of 540 nm. The operating wavelength is 1310 nm and the refractive index of MoS_2 is ∼4.2.[31] Inset: Scanning electron micrograph (SEM) of the portion of ultrathin MoS_2 pillars. The sample was covered with 5 nm thick gold to minimize charging. Scale bar: 500 nm. (h) Intensity profile measured along the axial plane of the MoS_2 metalens with an incident wavelength of 1310 nm. (i) Normalized intensity profile measured along the focal plane at 300 μm in panel h and its corresponding Gaussian fit.

rely on phase accumulation from the variable thickness or provide binary phase shifts. Varying the thickness in this manner necessitates the use of low-throughput fabrication technology, such as focused ion-beam milling. Lenses with binary phase shift are also less efficient.

In this paper, we design and fabricate the first vdW metalenses, with significantly reduced thickness (∼0.1λ to 0.5λ) compared with the optical wavelength, by exploiting the incomplete phase-based design approach[26,27] and the high refractive indices of vdW materials. We validate our design via the fabrication and characterization of metalenses at visible and near-infrared wavelengths. Because of the nature of vdW interactions, our proposed metalenses can be readily transferred onto diverse material platforms (Figure 1a), distinct from typical dielectric metasurfaces, limited by bottom-up material growth.

To design the metalenses, we first compute the transmission properties of periodic arrays of cylindrical vdW nanopillars using rigorous coupled-wave analysis (RCWA).[28] The pillars are made of wide-band-gap h-BN ($E_g \approx 5.2$ eV, refractive index

DOI: 10.1021/acs.nanolett.8b02875
Nano Lett. 2018, 18, 6961−6966

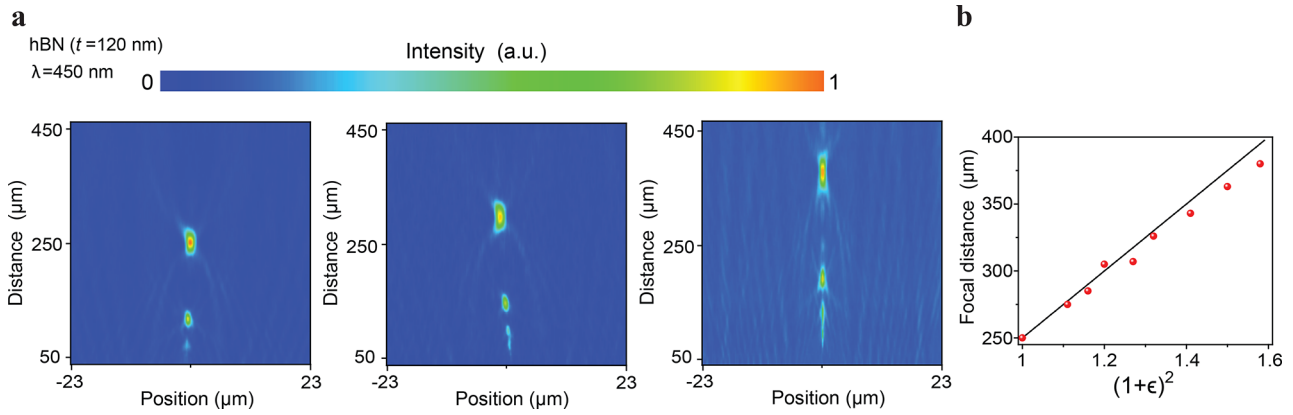

Figure 3. Integrable and tunable metalenses based on vdW materials. (a) Three representative intensity profiles measured along the axial plane of h-BN metalens integrated onto a PDMS substrate. Left to right: The strain applied to the PDMS substrate is 0, 9.5, and 25.6%, respectively. (b) Measured (round symbols) and analytically predicted (solid line) focal lengths under different strain values.

$n \approx 2.17$)[29] and rest on a quartz substrate with a lattice periodicity of $p \approx 260$ nm (Figure 1b). The wavelength of incident light is $\lambda = 450$ nm. By varying the dimensions of the pillars (thickness, t, and diameter, D), the transmitted light's phase and amplitude can be tuned (Figure 1c−e). This optical response can be explained by considering each pillar as a low-quality-factor Fabry−Perot resonator. The propagation phase increases with the dimensions of the resonator and varies rapidly near the supported resonant modes. On the basis of the selected dielectrics and designed parameters, the pillars should be thicker than 450 nm to achieve a complete 2π phase control.

To reduce the thickness of the scatterers while mitigating their drop in performance, we adopt the theory of incomplete phase modulation, originally developed for creating efficient liquid-crystal Fresnel optics.[26,27] For a spherical singlet lens, the addressed phase (φ) profile should follow

$$\varphi(r) = -\frac{\pi r^2}{\lambda F} \tag{1}$$

where r, λ, and F are the radial coordinate, optical wavelength, and focal length of the designed lens, respectively. With limited phase coverage, that is, the maximum phase shift being less than 2π (Figure 2a), the implemented phase functions can be correlated with the addressed $0-2\pi$ phase (φ) via a saturated mismatched model (Figure 2b,c, green curves, see the Supporting Information). This model is derived from the minimum Euclidean distance principle and should lead to higher focusing efficiency[27,30] compared with a simple linear interpolation (Figure 2b,c, blue curves; see the Supporting Information).

To experimentally demonstrate this concept, we design multiple metalenses with their D/f ranging from 0.3 to 0.4, where D and f are the diameter and focal length of the lens, respectively. To begin with, a 245 nm thick (~0.54 λ) exfoliated h-BN flake was transferred onto a quartz substrate and then patterned into an array of pillars to form four different metalenses with a focal length of $F = 160$ μm at $\lambda = 450$ nm (see the Supporting Information) and a lens diameter of 60 μm. Among them, lenses A and C comprise pillars that can only implement a phase shift range of 0.7π, whereas lenses B and D have a more limited phase modulation depth, a range of 0.5π (Figure 2d). Metalenses C and D are designed using linear interpolation (following Figure 2b,c, blue curves), whereas A and B are developed with the saturated mismatched model (following Figure 2b,c, green curves). We measure the focusing performance of the metalenses using the experimental setup schematically illustrated in Figure S1. Figure 2e,f shows the intensity profile measured in the designed focal plane. Despite the limited range of the implemented phase, all four lenses exhibit focusing. The corresponding intensity cuts through the center of their focal spots show that the full width at half-maximum (fwhm) for all of the metalenses is ~2.8 μm, close to the diffraction-limited fwhm of 2.3 μm. Moreover, the focusing from metalenses B and C indicates that metalenses developed with the saturated mismatched model (lens B) with smaller phase modulation can have higher focal intensity than a lens (lens C) developed using the linear interpolation model, even with a larger phase modulation depth (Figure 2f). Specifically, we found that in using the saturated mismatched model, the focusing efficiency could be increased by ~1.5 times while having the same phase modulation. We note that these results not only agree with our numerical simulations but also indicate the possibility of creating thin and efficient dielectric lenses with limited phase coverage (see Figure S2 and Table S1). Thus with this design principle we can relax the stringent requirements on the scatterers to reach a full 2π phase shift. This, in turn, avoids the necessity of fabricating high-aspect-ratio structures and provides better tolerance to fabrication and simulation errors.

To extend the metalenses to a longer wavelength regime, we use TMDC, specifically molybdenum disulfide (MoS_2), to make metalenses. MoS_2 has a high refractive index[31] that in combination with incomplete phase design can potentially push the thickness of dielectric metalenses to far below the operating wavelength. To verify this concept, we fabricated a metalens based on 190 nm thick (~0.14 λ) MoS_2 pillars with a designed focal length of 300 μm and a lens diameter of 100 μm. The simulated optical response of arrays of MoS_2 pillars at $\lambda = 1310$ nm is shown in Figure 2g, and the phase profile of the lens was developed using the saturated mismatch model with the implemented phase shift ranging from 0 to 0.7π. By using the characterization setup shown in Figure S1, we can examine the intensity profile of this designed lens and resolve a near-diffraction-limited focal spot (fwhm ~5 μm) at $F = 300$ μm (Figure 2h,i), which agrees with our design parameters, showing the promise for achieving a compact infrared imaging system.

DOI: 10.1021/acs.nanolett.8b02875
Nano Lett. 2018, 18, 6961−6966

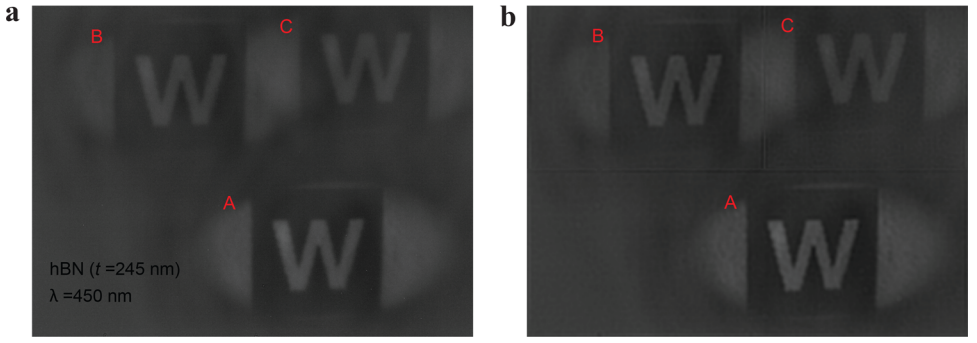

Figure 4. vdW metalenses for optical imaging application. (a) Images formed by metalens A (bottom), B (top left), and C (top right), simultaneously captured using a CMOS imaging sensor. (b) Same images shown in panel a after computational postprocessing. The "W" in the images is used with permission from the University of Washington.

With the success of our as-fabricated devices for focusing, we next explore the integrability of vdW metalenses in systems. In this experiment, a 120 nm thick exfoliated h-BN flake was patterned into a metalens with focal length F = 250 μm on a quartz substrate (see Figure S6). This prepatterned device was subsequently transferred onto a stretchable polydimethylsiloxane (PDMS) substrate using the dry-transfer pick-up technique.[15,16] To characterize the optical properties and tunability of the transferred device, we resolve the transmitted light intensity profiles along the axial plane as a function of radial strain applied to the PDMS (Figure 3a). In the absence of strain, the focal length of the lens is at the designed 250 μm, suggesting that the metalens remains intact after the transfer procedure. In addition to the focal spot at F, multiple high-intensity spots can be observed at F/N, where N is an integer. This behavior originates from the incomplete phase implementation (see Figures S3 and S4). In applying the radial strain (ϵ), the measured focal spot shifts away from the initial focal plane of the metalens (see the Supporting Information). This tuning behavior is linearly proportional to $(1 + \epsilon)^2$ (Figure 3b), which not only agrees with the theoretical prediction[32,33] but also highlights the opportunities of utilizing vdW materials for making tunable metasurfaces.

Finally, we examine the efficacy of the design and fabrication process by capturing images with the h-BN metalenses in Figure 2d using a custom-built imaging system (Figure S1). The scattered light from a printed University of Washington logo ("W") is captured using metalenses A, B, and C, which were imaged by a CMOS camera (Figure 4a). Critically, these results demonstrate that our proof-of-concept devices can form images. Metalens A, designed via the saturated mismatched model, exhibits superior performance relative to the other two, evidenced by its greater luminance and sharpness. This is consistent with the fact that the saturated mismatched model is more efficient compared with the linear mismatched model, which generates a lower intensity image. We note that this imaging quality can be further improved by using computational postprocessing[34] (Figure 4b; see Figure S5) or by increasing the numerical aperture of the metalenses (Figure S8), making our developed thin metalenses more attractive for imaging applications.

In summary, we demonstrated a viable route to realize ultrathin dielectric metalenses based on vdW materials. This adapted design principle can be applied to different spectral regions, a broad class of dielectric materials, and circumvents the current fabrication challenge of making high-aspect-ratio nanoscale scatters. In particular, ultrathin and high-numerical-aperture metalenses can theoretically be realized by using high-index TMDCs[35,36] and perform better than typical Si, TiO_2, or Si_3N_4 metalenses.[11] However, it is notable that high-index materials would have a smaller band gap and thus higher absorption losses, resulting in limited applicable wavelength range. Additionally, we show that utilizing vdW materials would offer a unique opportunity to realize metalenses that are integrable with other substrates, including flexible polymers. It is also noteworthy that many emerging layered materials exhibit diverse optical properties, such as anisotropy, phase-change, or nonlinear behaviors, and such materials could be further stacked together to form more complicated vdW heterostructures with the ability to tailor material properties with atomic precision.[15] These new material properties, along with the large area growth of vdW materials[37,38] and patterning via stepper photolithography,[39,40] thus present a tremendous potential for creating vdW metasurfaces with novel functionalities for applications in optical sensing, imaging, polarimetry, focal length tuning, and energy harvesting.

■ ASSOCIATED CONTENT

Supporting Information

The Supporting Information is available free of charge on the ACS Publications website at DOI: 10.1021/acs.nanolett.8b02875.

Detailed measurement setup and procedure, device fabrication, design parameters of metalenses, modeling of incomplete phase design, focusing efficiency, stretchable metalens, improving the quality of optical imaging. (PDF)

■ AUTHOR INFORMATION

Corresponding Authors

*C.-H.L.: E-mail: chliu@ee.nthu.edu.tw.
*A.M.: E-mail: arka@uw.edu.

ORCID

Jiajiu Zheng: 0000-0003-1527-201X
Yueyang Chen: 0000-0002-4390-550X
Arka Majumdar: 0000-0003-0917-590X

Author Contributions

⊥J.Z. and S.C. contributed equally. C.-H.L. and A.M. conceived the idea. C.-H.L. and S.C. performed the design and simulation. J.Z. fabricated all of the devices. T.K.F. and Y.C. helped with material search and AFM characterization. C.-H.L.

DOI: 10.1021/acs.nanolett.8b02875
Nano Lett. 2018, 18, 6961−6966

performed the measurement and data analysis with help from S.C. X.X. and A.M. supervised the whole project.

Notes

The authors declare no competing financial interest.

■ ACKNOWLEDGMENTS

We acknowledge Mr. Alan Zhan for input on fabrication. This work is supported by the AFOSR grant FA9550-18-1-0104 (program manager Dr. Gernot Pomrenke), NSF MRSEC 1719797, and the Ministry of Science and Technology of Taiwan under grant MOST 107-2112-M-007-002-MY3. All of the fabrication processes were performed at the Washington Nanofabrication Facility (WNF), a National Nanotechnology Infrastructure Network (NNIN) site at the University of Washington, which is supported in part by the National Science Foundation (awards 0335765 and 1337840), the Washington Research Foundation, the M. J. Murdock Charitable Trust, GCE Market, Class One Technologies and Google.

■ REFERENCES

(1) Wu, C. H.; Neuner, B., III; John, J.; Milder, A.; Zollars, B.; Savoy, S.; Shvets, G. *J. Opt.* **2012**, *14*, 024005.
(2) Kildishev, A. V.; Boltasseva, A.; Shalaev, V. M. *Science* **2013**, *339*, 1232009.
(3) Yu, N. F.; Capasso, F. *Nat. Mater.* **2014**, *13*, 139−150.
(4) Arbabi, A.; Horie, Y.; Bagheri, M.; Faraon, A. *Nat. Nanotechnol.* **2015**, *10*, 937−943.
(5) Jahani, S.; Jacob, Z. *Nat. Nanotechnol.* **2016**, *11*, 23−36.
(6) Yu, N. F.; Genevet, P.; Kats, M. A.; Aieta, F.; Tetienne, J. P.; Capasso, F.; Gaburro, Z. *Science* **2011**, *334*, 333−337.
(7) Ni, X. J.; Ishii, S.; Kildishev, A. V.; Shalaev, V. M. *Light: Sci. Appl.* **2013**, *2*, e72.
(8) Aieta, F.; Genevet, P.; Kats, M. A.; Yu, N. F.; Blanchard, R.; Gaburro, Z.; Capasso, F. *Nano Lett.* **2012**, *12*, 4932−4936.
(9) Meinzer, N.; Barnes, W. L.; Hooper, I. R. *Nat. Photonics* **2014**, *8*, 889−898.
(10) Chen, H. T.; Taylor, A. J.; Yu, N. F. *Rep. Prog. Phys.* **2016**, *79*, 076401.
(11) Genevet, P.; Capasso, F.; Aieta, F.; Khorasaninejad, M.; Devlin, R. *Optica* **2017**, *4*, 139−152.
(12) Khorasaninejad, M.; Chen, W. T.; Devlin, R. C.; Oh, J.; Zhu, A. Y.; Capasso, F. *Science* **2016**, *352*, 1190−1194.
(13) Zhan, A.; Colburn, S.; Trivedi, R.; Fryett, T. K.; Dodson, C. M.; Majumdar, A. *ACS Photonics* **2016**, *3*, 209−214.
(14) Xia, F. N.; Wang, H.; Xiao, D.; Dubey, M.; Ramasubramaniam, A. *Nat. Photonics* **2014**, *8*, 899−907.
(15) Novoselov, K. S.; Mishchenko, A.; Carvalho, A.; Castro Neto, A. H. *Science* **2016**, *353*, aac9439.
(16) Liu, Y.; Weiss, N. O.; Duan, X. D.; Cheng, H. C.; Huang, Y.; Duan, X. F. *Nature Rev. Mater.* **2016**, *1*, 16042.
(17) Geim, A. K.; Grigorieva, I. V. *Nature* **2013**, *499*, 419−425.
(18) Sun, Z. P.; Martinez, A.; Wang, F. *Nat. Photonics* **2016**, *10*, 227−238.
(19) Liu, C. H.; Clark, G.; Fryett, T.; Wu, S. F.; Zheng, J. J.; Hatami, F.; Xu, X. D.; Majumdar, A. *Nano Lett.* **2017**, *17*, 200−205.
(20) Jariwala, D.; Davoyan, A. R.; Wong, J.; Atwater, H. A. *ACS Photonics* **2017**, *4*, 2962−2970.
(21) Li, Y. Z.; Zhang, J. X.; Huang, D. D.; Sun, H.; Fan, F.; Feng, J. B.; Wang, Z.; Ning, C. Z. *Nat. Nanotechnol.* **2017**, *12*, 987−992.
(22) Kim, S.; Froch, J. E.; Christian, J.; Straw, M.; Bishop, J.; Totonjian, D.; Watanabe, K.; Taniguchi, T.; Toth, M.; Aharonovich, I. *Nat. Commun.* **2018**, *9*, 2623.
(23) Li, P. N.; Dolado, I.; Alfaro-Mozaz, F. J.; Casanova, F.; Hueso, L. E.; Liu, S.; Edgar, J. H.; Nikitin, A. Y.; Velez, S.; Hillenbrand, R. *Science* **2018**, *359*, 892−896.
(24) Yang, J.; Wang, Z.; Wang, F.; Xu, R. J.; Tao, J.; Zhang, S.; Qin, Q. H.; Luther-Davies, B.; Jagadish, C.; Yu, Z. F.; Lu, Y. R. *Light: Sci. Appl.* **2016**, *5*, e16046.
(25) Kong, X. T.; Khan, A. A.; Kidambi, P. R.; Deng, S.; Yetisen, A. K.; Dlubak, B.; Hiralal, P.; Montelongo, Y.; Bowen, J.; Xavier, S.; Jiang, K.; Amaratunga, G. A. J.; Hofmann, S.; Wilkinson, T. D.; Dai, Q.; Butt, H. *ACS Photonics* **2015**, *2*, 200−207.
(26) Moreno, I.; Campos, J.; Gorecki, C.; Yzuel, M. J. *J. Jpn. J. Appl. Phys.* **1995**, *34*, 6423−6432.
(27) Moreno, I.; Iemmi, C.; Marquez, A.; Campos, J.; Yzuel, M. *Appl. Opt.* **2004**, *43*, 6278−6284.
(28) Liu, V. F.; Fan, S. *Comput. Phys. Commun.* **2012**, *183*, 2233−2244.
(29) *Properties of Advanced Semiconductor Materials*; Levinshtein, M. E.; Rumyantsev, S. L.; Shur, M. S., Eds.; Wiley: New York, 2001.
(30) Juday, R. D. *Appl. Opt.* **1993**, *32*, 5100−5111.
(31) Beal, A. R.; Hughes, H. P. *J. Phys. C: Solid State Phys.* **1979**, *12*, 881−890.
(32) Kamali, S. M.; Arbabi, E.; Arbabi, A.; Horie, Y.; Faraon, A. *Laser Photon. Rev.* **2016**, *10*, 1002−1008.
(33) Ee, H. S.; Agarwal, R. *Nano Lett.* **2016**, *16*, 2818−2823.
(34) Colburn, S.; Zhan, A.; Majumdar, A. *Science Adv.* **2018**, *4*, eaar2114.
(35) Yang, J. J.; Fan, J. A. *Opt. Express* **2017**, *25*, 23899−23909.
(36) Bayati, E.; Zhan, A.; Colburn, S.; Majumdar, A. The Role of Refractive Index in Metalens Performance. 2018, arXiv:1805.04659 [physics.optics]. arXiv.org e-Print archive. https://arxiv.org/abs/1805.04659.
(37) Kang, K.; Xie, S. E.; Huang, L. J.; Han, Y. M.; Huang, P. Y.; Mak, K. F.; Kim, C. J.; Muller, D.; Park, J. *Nature* **2015**, *520*, 656−660.
(38) Kang, K.; Lee, K. H.; Han, Y. M.; Gao, H.; Xie, S. E.; Muller, D. A.; Park, J. *Nature* **2017**, *550*, 229−233.
(39) Colburn, S.; Zhan, A.; Majumdar, A. *Optica* **2018**, *5*, 825−831.
(40) She, A.; Zhang, S. Y.; Shian, S.; Clarke, D. R.; Capasso, F. *Opt. Express* **2018**, *26*, 1573−1585.
(41) Hail, U. C.; Poulikakos, D.; Eghlidi, H. High-Efficiency, Extreme-Numerical-Aperture Metasurfaces Based on Partial Control of the Phase of Light. 2018, arXiv:1807.06997 [physics.optics]. arXiv.org e-Print archive. https://arxiv.org/abs/1807.06997.

■ NOTE ADDED IN PROOF

During the peer review of the manuscript, another paper was published, where partial phase is used to create high-numerical-aperture lenses.[41]

DOI: 10.1021/acs.nanolett.8b02875
Nano Lett. 2018, 18, 6961−6966